fire

Article

Enhancing Fire Monitoring Method over Peatlands and Non-Peatlands in Indonesia Using Visible Infrared Imaging Radiometer Suite Data

Andy Indradjad [1,2], Muhammad Dimyati [1,*], Yenni Vetrita [2], Erna Sri Adiningsih [2] and Rokhmatuloh Rokhmatuloh [1]

[1] Faculty of Math and Sciences, University of Indonesia, Depok 16424, Indonesia; andy003@brin.go.id (A.I.); rokhmatuloh.ssi@ui.ac.id (R.R.)
[2] Remote Sensing Research Center, National Research and Innovation Agency, Cibinong 16911, Indonesia; yenni.vetrita@brin.go.id (Y.V.); rrer001@brin.go.id (E.S.A.)
* Correspondence: m.dimyati@sci.ui.ac.id

Abstract: Indonesia needs a daily monitoring system due to its frequent fires and, more importantly, to assist stakeholders in the field in taking action to mitigate disasters. Our method simplified the number of hotspots for field-based purposes and was verified by comparing the point-based (point-HS) VIIRS (Visible Infrared Imaging Radiometer Suite) 375m-derived temperature anomalies (hotspots) and clustered-based hotspots (cluster-HS, our suggested method). Using Euclidean clustering, we calculated the distance between hotspot points and applied specific criteria to reduce the number of hotspots while aligning them closely with fire incidents. We evaluated accuracy at different fire sizes, burned areas, peatlands, and distances from the reported burn center. We found that the accuracy increases at 1.5 km from the center of the fire for both point- and cluster-HS at 52% and 53%, respectively. For areas larger than 14 ha, both types of hotspots yielded superior results of 83%. Cluster-HS performs better on peatlands than non-peatlands (62% vs. 57%). Without diminishing the precision of the hotspot observation, this study indicates that our method is reliable for assisting field stakeholders in the field in taking actions. Therefore, this product could be implemented into Indonesia's daily hotspot monitoring.

Keywords: VIIRS; active fire; clustering method; fire management; peatland

check for updates

Citation: Indradjad, A.; Dimyati, M.; Vetrita, Y.; Adiningsih, E.S.; Rokhmatuloh, R. Enhancing Fire Monitoring Method over Peatlands and Non-Peatlands in Indonesia Using Visible Infrared Imaging Radiometer Suite Data. *Fire* **2024**, *7*, 9. https://doi.org/10.3390/fire7010009

Academic Editors: Fuquan Zhang, Ting Yun, António Bento-Gonçalves and Luis A. Ruiz

Received: 24 November 2023
Revised: 17 December 2023
Accepted: 20 December 2023
Published: 23 December 2023

1. Introduction

Forest and land fires are recurrent disasters in Indonesia that have had significant impacts, particularly in 2015, and caused an estimated loss of up to USD 16 billion [1]. These fires can potentially impact air quality, as was the case with those in Sumatra and Kalimantan in particular, which have had consequences for the air quality of neighboring countries [2]. Fires emit toxic gasses into the atmosphere, including carbon dioxide and carbon monoxide [3]. The long-term effects of these fires can be detrimental to the cardiovascular system, respiratory health, mortality rates, and even the height of individuals [4–7].

The consequences of fires are already well known, yet pinpointing fire sources or affected areas remains challenging. These are critical for national fire management in a large archipelagic country. Indonesia requires effective techniques to address its fire management needs. Remote sensing technology has been extensively employed to identify hotspots and areas impacted by fires [8–10].

The detection of temperature anomalies on the Earth's surface (hereafter referred to as hotspot) is one of the most useful and widely used approaches, usually involving data derived from satellite imagery. The thermal sensors on satellites such as Terra/Aqua MODIS (Moderate-Resolution Imaging Spectroradiometer), NOAA/METOP AVHRR (Advanced Very-High-Resolution Radiometer), and Himawari-8 AHI (Advanced Himawari

Imager) has enabled the development of a global algorithm for locating any hotspots [11,12]. These data are derived from imagery with a low spatial resolution (375–2000 m). However, adapting Himawari-8 to produce data multiple times per day or every 10 min would allow for more frequent observations. They are suitable for near-real-time fire monitoring. In addition to high temporal observation [13,14], these satellites cover the globe and have the ability to provide consistent and automatic hotspot data. The availability of long-term data [15] makes them suitable for climate change-related topics as well.

The advancement of global hotspot algorithm development, typified by the MODIS Collection 6 product [16], has increased the probability of detecting tropical fires and decreased the number of false alarms. This algorithm employs a wavelength of 4 and 11 μm [17]. The SNPP (Suomi National Polar-orbiting Partnership) and NOAA-20 satellites, which are the replacements for Terra/Aqua MODIS, continue to generate reliable hotspots [18] with a higher spatial resolution (375 m and 750 m) [19] than their predecessor (MODIS, 1 km) [18]. Visible Infrared Imaging Radiometer Suite (VIIRS) night-time data could analyze the subpixel using the Planck curve fitting technique [19,20], allowing for the rapid mapping of burned areas [21,22]. Hotspots are also necessary inputs for producing burned maps using various methods [23–25]. At medium resolution, thanks to Landsat 8 and Sentinel-2, which have an Operational Land Imager (OLI) sensor and Multispectral Instrument (MSI), respectively, hotspots can also be derived by employing Shortwave Infrared bands [26,27]. Because their resolution is as low as five days, however, these satellites are not ideal for more frequent monitoring.

Recent increases in the abundance of hotspot data raise the question of whether this aids or hinders fire management in the field. To our knowledge, there have been no detailed discussions on this in Indonesia. In addition, the types of fires in Indonesia are not similar to those in other countries, where the size of many fires is small and tends to underestimate hotspots, not only because of their size but also because of persistent clouds [28]. The Indonesian government is attempting to control fires, particularly in areas across the country that are prone to fires and smoke. Hotspots have become the main avenue for field checking. More hotspots imply that more locations must be investigated. Thus, a strategy to decide which hotspots should be investigated must be developed using a reliable approach.

Global algorithms are designed to produce reliable results across different regions by reducing sensitivity in certain areas while preserving consistency in others. However, the variation in fire regimes across the globe may be unique and necessitate a particular focus on identifying biomass burning [29]. To this end, persistent anomalies originating from non-biomass burning activities, such as volcano activity, road, settlement, offshore and water bodies [30], can be eliminated [31–33].

Another technique for dealing with how to simplify which hotspots should be checked first is to use spatial clustering hotspots by, for example, using the Euclidean distance method. Clustering can be performed both spatially and temporally [11,34–42]. Among the techniques used for this are K-mean, Fuzzy-C Means, and Linkage [39,43,44], as well as the Poisson Method [45] and Density-Based Spatial Clustering Algorithm with Noise (DBSCAN) [46–49]. However, they have not yet been used for daily fire monitoring, as they predominantly focus on analyzing archive data to identify fire-prone regions.

The development of fire detection and monitoring methods is still lacking in certain areas to fulfill the need for rapid responses and the ground checking of any fire occurrence in the field. The existing methods using high resolution data [50,51] can present detailed information on fire events, but they cannot be applied for daily fire monitoring. On the other hand, fire detection or monitoring using low spatial resolution data usually produces several points over large fire areas [33,52]. The large number of fire points could lead to more efforts in preparing a quick response in the field. Therefore, there is an urgent need to develop or enhance the method by clustering the fire points to reduce the number of locations to be checked in the field. Clustering methods could be developed using various approaches. Among these methods is Euclidean distance, which is the simplest one to apply to daily satellite data for fire monitoring.

The use of vision-based methods should be more intuitive to detect fire and burned areas by image processing or machine learning methods [53,54]. Vision-based methods are widely used and serve as a typical method for detecting both fires and burned areas [55]. However, this study did not use high-spatial-resolution data due to low temporal resolution. This limitation could not fulfil the need for daily fire monitoring. In addition, fire behavior can be site-specific.

This study attempts to fill this gap. We aimed to develop and evaluate the effectiveness of the VIIRS 375m-derived hotspot clustering method, using the present situation in Indonesia as a case study. We used the Euclidean clustering method by calculating the distance between the points of hotspots and applying specific criteria to minimize the number of hotspots while aligning them closely with actual fire incidents. Our findings are expected to be able to assist relevant stakeholders in planning field actions, such as deciding which location should be investigated first based on an understanding of fire consequences.

2. Materials and Methods

2.1. VIIRS Data Product Description

The characteristics of the VIIRS sensor aboard the SNPP and NOAA-20 satellites are essentially identical; in fact, it outperforms those of the MODIS sensor. This sensor can be used to obtain hotspot information [18]. To obtain hotspot information, band M13 and M15 VIIRS data, which have wavelengths of 3.973–4.128 and 10.263–11.263 μm, respectively, with a moderate resolution of 750 m were used. This algorithm operates at a resolution of 375 m by utilizing bands I4 and I5, which have wavelengths of 3.55–3.93 and 10.5–12.4 μm [56]. The performance of this algorithm can also provide additional information about the affected area [21]. Although the radiometric characteristics of VIIRS data obtained from the SNPP and JPSS (Joint Polar Satellite System) satellites may slightly differ, they share similarities [57]. The processing of VIIRS data utilizes the Community Satellite Processing Package (CSPP), a data processing software developed by the University of Wisconsin. This software can process data through various stages, from raw data records to active fires, using separate processing modules [58]. Furthermore, to enable automatic integration, it is necessary to develop a system that connects these processing modules [59].

We used the VIIRS active fire global product algorithm (see [56] for more details), which can be ran using VIIRS AF Software Version 1.1.1. from the CSPP (Community Satellite Processing Package) [33,58,60]. Input data were obtained from the Parepare ground station, which was previously managed by the Indonesian National Institute of Aeronautics and Space (LAPAN) (currently merged into the National Research and Innovation Agency). From this running program, the initial information generated consists of location (latitude/longitude), time, confidence level, and satellite source data. For national interests, we added information on administrative location and radius of possibility (see detail in Section 2.3.1). The radius of possibility is 3 times the sensor resolution (3×375 m). This number was chosen to anticipate inaccuracies in spatial resolution because sensor resolution is a measure of the nadir position, whereas off-nadir can be several times lower than the resolution at nadir. In addition, since the product focuses on vegetation fires, the product excluded the persistent anomaly provided by [32]. From this point forward, all hotspot data generated by this product will be referred to as point-HS.

2.2. Data Types and Sources

2.2.1. Field Data and the Burned Area Map

Fire information encompassing all provinces in Indonesia (Figure 1) was gathered using field data and a burned area map. Both were acquired from the Ministry of Environment and Forestry (MoEF) of the Republic of Indonesia. Field data consisted of suppression or ground truth points concerning fire incidents compiled from 1 January to 30 November 2020. The data provide specific information regarding the rough estimated burned areas, dates, and coordinates. During that period, a total of 1881 fire occurrences were documented, with the majority (80%) resulting in burns of less than 3.5 hectares (see Table 1).

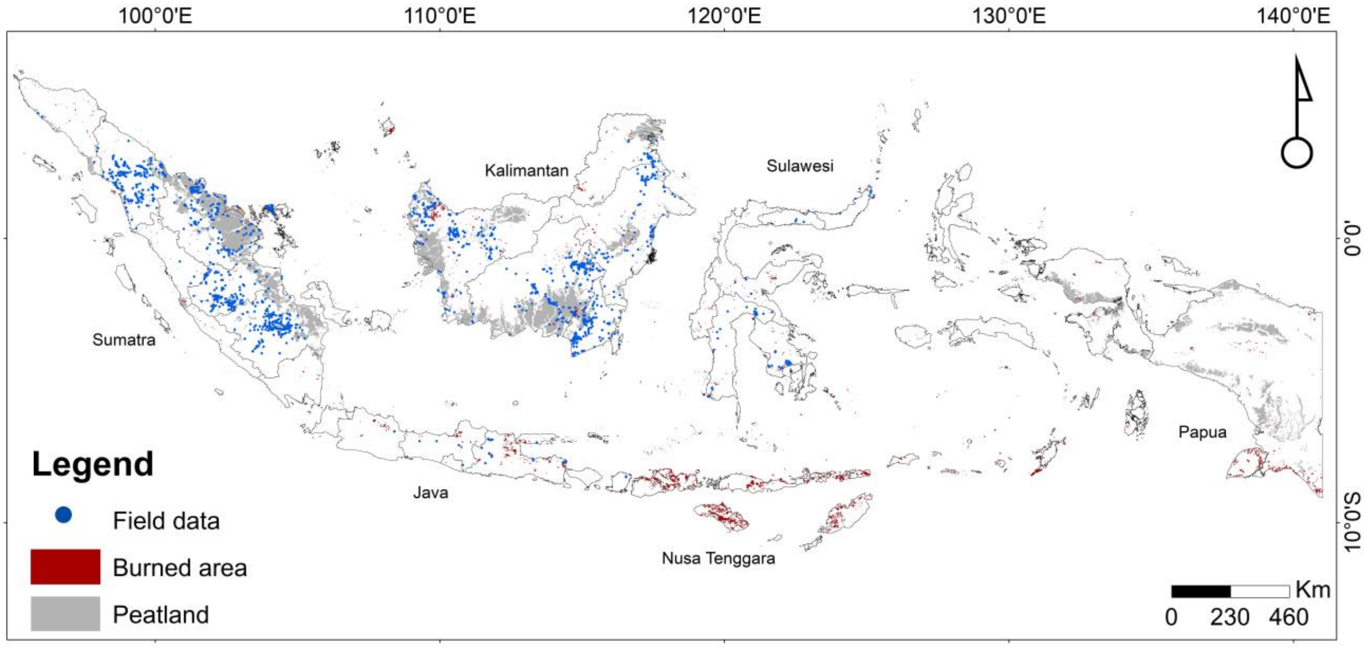

Figure 1. Distribution map of field data, burned areas, and peatlands.

Table 1. Summary of field data overlaid on maps of burned areas and peatlands.

Estimation of Burn Area (ha)	Field Data (%)	Burn Area Map (%)	Number of Points in Peatlands Only	Number of Points in Non-Peatlands Only
≤3.5	80.06	25.16	318	1188
>3.5	19.94	74.84	169	206
>7.0	9.14	57.93	95	77
>14.0	4.04	41.65	47	29

Burned area maps, on the other hand, are represented as polygons and include detailed information such as the size of each fire event and the specific images used to create the map. The MoEF made this national-scale map from Landsat 8 images (30 m resolution) primarily by visual interpretation. The shapefile data are now inaccessible to the public; however, the key statistics can be obtained by downloading them from the official website of the MoEF (https://sipongi.menlhk.go.id/, accessed on 1 August 2023). Among the 1881 field locations, only around 473 points were identified by the burned area map (Table 1), primarily concentrated in areas affected by large fires. It should be noted that only a quarter of small fires (with an area ≤ 3.5 hectares) are incorporated into the map. Table 1 provides a comprehensive summary of the field data in conjunction with the burned area and peatland maps that are of critical interest to us.

2.2.2. Peatland Map

We used the 2011 version of the peatland map provided by the Ministry of Agriculture of the Republic of Indonesia [61]. According to this map, peatland occupied around 11.2 million hectares of land in Indonesia. Out of the 1881 field data points, 26% were in peatlands. The peatland map consists of polygons.

2.3. Research Method

Figure 2 shows the overall research design. The following subsection explains the details for each step. All available VIIRS I-band images from 2020 at SDR (Science Data Record) level were processed for further analysis.

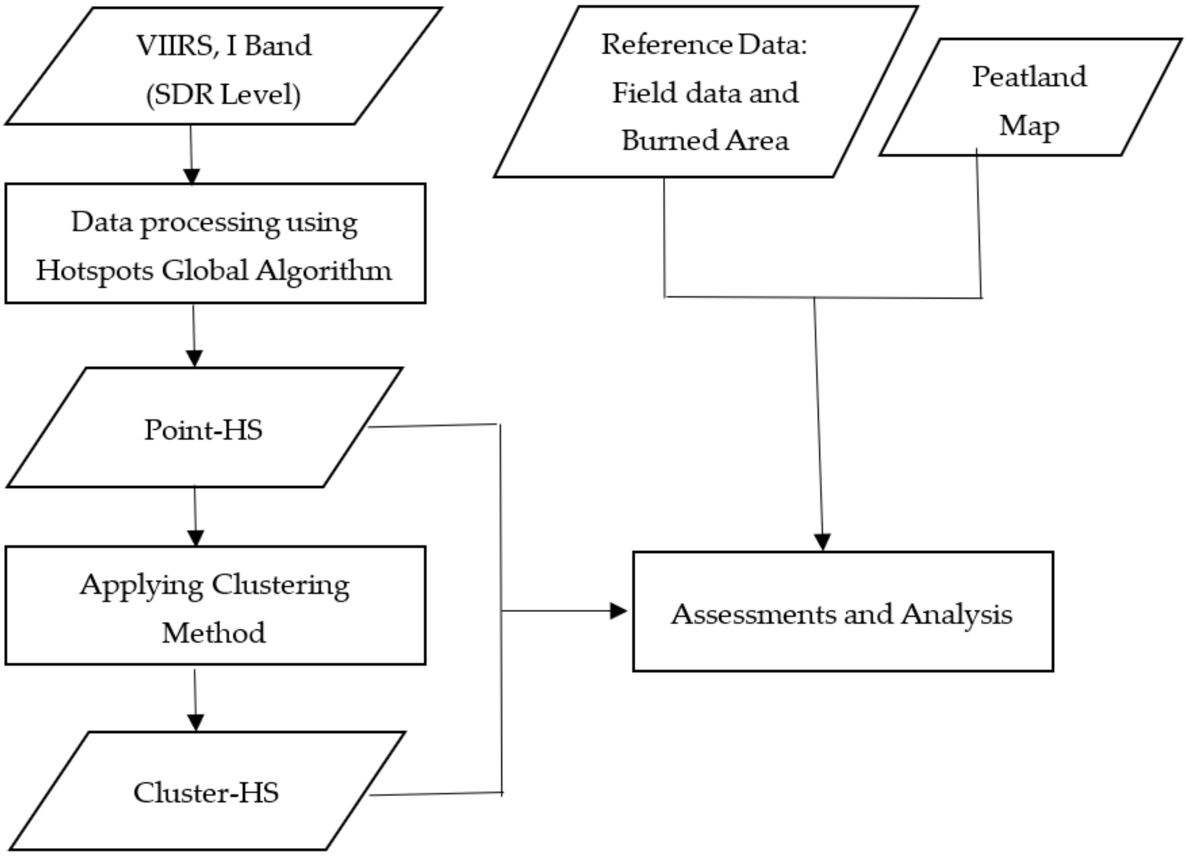

Figure 2. Research design. Visible Infrared Imaging Radiometer Suite (VIIRS) I-band images (375 m) at Science Data Record (SDR) level were the main input data, as required by the global product algorithm [58]. Maps of burned areas, peatlands, and field data were used to evaluate the proposed clustered hotspots (cluster-HS).

2.3.1. Hotspot Clustering Method

The hotspot clustering method (hereinafter, cluster-HS) initially involved reading the list of point-based hotspots (hereinafter, point-HS), per satellite per time, to be clustered. Point-HS refers to hotspot information derived using the global algorithm [56]. All point-HS has information such as coordinates (latitude/longitude), level of confidence values, administrative location data, and radius of possibility data. Figure 3 shows a flowchart of the clustering method, along with an illustration; the following paragraphs explain each part of the method.

The following steps involve selecting hotspot points and calculating the Euclidean distance (d) between points. The Euclidean distance was calculated using Equation (1):

$$d = \sqrt{(x_1 - x_2)^2 + (y_1 - y_2)^2} \quad (1)$$

where

$$d = distance\ (\mathrm{m})$$

$$x_1, y_1 = Coordinates\ (latitude\ and\ longitude)\ of\ first\ point$$

$$x_2, y_2 = Coordinates\ of\ second\ point$$

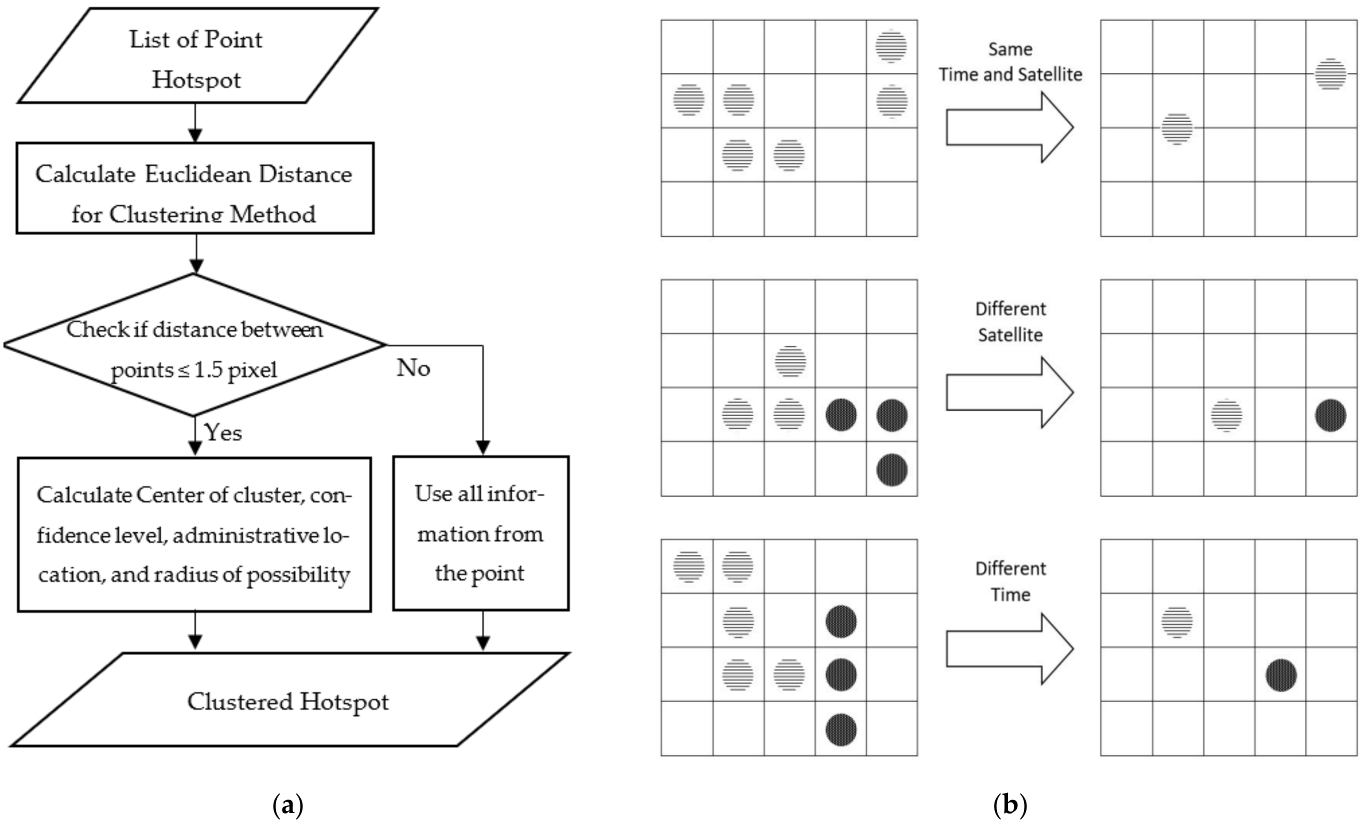

Figure 3. Clustering method (**a**) and illustration (**b**).

The Euclidean distance between each selected hotspot point and other points was calculated. It searched for hotspot points in its vicinity that met specific distance criteria, where the distance (d) satisfied the criteria described in Equation (2):

$$0 < d \leq 1.5p \tag{2}$$

where

$$d = \text{distance between point (m)}$$

$$p = pixel(ground)resolution\ (375\ \text{m})$$

When other hotspot points met the criteria, they were included in the same group. This step involved calculating the distance between the selected points and other points and searching for hotspot points around them that met the specified requirements. The process was repeated for all other hotspot points to determine cluster groups. Once the cluster groups were formed, the next step involved calculating the center coordinates of the clusters, their levels of confidence, their administrative locations, and the radii of possibility for the clusters. The center coordinates of the clusters were calculated using the formula described in Equation (3):

$$x_c = \frac{\sum_{i=1}^{n} x_i}{n} \qquad y_c = \frac{\sum_{i=1}^{n} y_i}{n} \tag{3}$$

where

$$n = number\ of\ cluster\ members$$

$$x_c, y_c = Coordinates\ (latitude\ and\ longitude)\ of\ cluster$$

$$x_i, y_i = Coordinates\ of\ any\ given\ points$$

The confidence levels (CLs) of the clusters were calculated by averaging all CL-point members within the clustered group using the formula described in Equation (4):

$$CL_c = \text{int}\left(\frac{\sum_{i=1}^{n} CL_i}{n}\right) \tag{4}$$

where

$$n = number\ of\ cluster\ members$$

$$CL_c = Confidence\ level\ of\ cluster\ (rounded)$$

$$CL_i = confidence\ level\ of\ cluster\ member\ pixel$$

The administrative locations of the clusters were calculated based on the mode of the administrative locations among the cluster members. The radii of possibility (RK) were determined using the formula described in Equation (5):

$$RK_c = \text{int}\left(p \times \left(\sqrt{n} + 2\right)\right) \tag{5}$$

where

$$n = number\ of\ clusters\ members$$

$$RK_c = radius\ of\ the\ possibility\ of\ a\ cluster\ (rounded)$$

$$p = pixel\ resolution\ (in\ this\ case\ 375\ \text{m})$$

2.3.2. Assessments and Analysis

To validate the hotspot data, low-resolution satellite data were compared with medium-resolution units [14,62,63]. For the low-resolution satellite data, an assessment was conducted using field data to facilitate a comparison [9,64], and this was necessary to evaluate the hotspot methods [65].

The field data were compared with VIIRS sensor hotspot units for the same period. Validation was performed by matching the coordinates in the field data with the hotspot database, considering date and distance criteria, using the Euclidean distance formula (Equation (1)). The date criteria include two days before and one day after the field data, labeled as detected since there was a hotspot in the database that met the criteria. The selection of the duration for this day was made considering the potential discrepancy between the date recorded in the field, as reported by officials, and the actual day of the fire's initiation. The success of this activity is contingent upon the availability of resources and the accessibility of fire locations. We adhered to a strict policy of selecting the day immediately after the field report's date to ensure accurate calculation and prevent any potential oversights. The distance buffer also needs to be used to compare locations based on the field data and hotspots [63]. The distance buffer was used because most of the ground truth data locations were collected about 0–2 km away from the fire area [66]. The distance buffer criteria range from a 1- to 10-pixel resolution (see Figure 4). The percentage of fire events detected by hotspots compared to the actual fire events was calculated using the following:

$$POD = \frac{NHS}{NT} \times 100\% \tag{6}$$

where

$$POD = Percentage\ of\ detection$$

$$NHS = number\ of\ fire\ event\ detected\ by\ hotspots$$

$$NT = number\ of\ total\ fire\ events\ in\ the\ field\ data$$

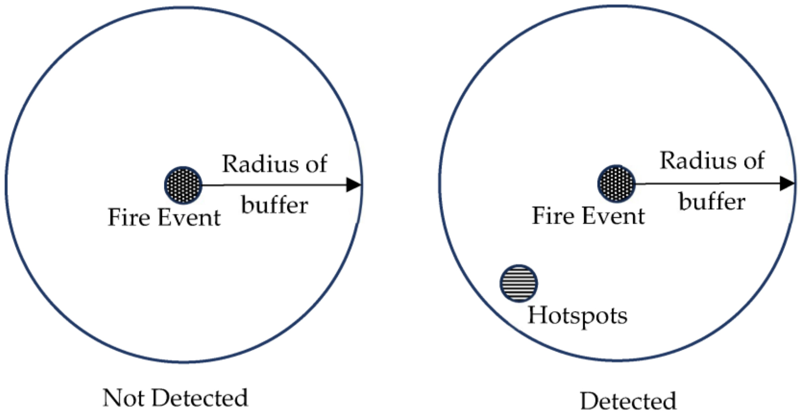

Figure 4. Illustration of fire events detected by hotspots.

To analyze the effectiveness of the buffer distance, the difference between the number of detected hotspots from each buffer criterion by subtraction was used, and this was calculated using the following:

$$Difference = NHS_n - NHS_{n-1} \quad (7)$$

where

$$NHS_n = number\ of\ fire\ event\ detected\ by\ hotspots\ at\ n$$

$$NHS_{n-1} = number\ of\ fire\ event\ detected\ by\ hotspots\ at\ n\ -\ 1\ (previous)$$

The optimal buffer distance for application was calculated by comparing two trend lines with clearly distinguishable slopes, with one being steep and the other sloping. The intersection was identified as the most favorable buffer distance.

3. Results

3.1. Cluster-HS Product

Examples of cluster-HS products are presented in Table 2. The cluster-HS method allows us to determine the number of neighborhoods in which the point-HS are identified as cluster-HS. In Table 2, for example, the radius is represented by the numerical value 1280, which signifies the origin of the cluster-HS from two points-HS (see Equation (5)). Based on Equation (5), a higher numerical value for *RK* indicates a higher number of cluster members. Cluster-HS preserves the point-HS derived from many satellite sources, enabling us to continuously monitor the original source of each point-HS.

Table 2. Examples of detailed information for each cluster-HS (*CL* = confidence level; *RK*= radius of possibility). In the "Method" column, the associated technique (cluster or point) is indicated.

Id	Date	Time	Latitude	Longitude	CL	Satellite	RK	Subdistrict	District	Province	Method
1	3 March 2020	00:52:43	−0.06421	103.1234	8	noaa20	1280	Gaunganakserka	Indragiri Hilir	Riau	Cluster
2	3 March 2020	00:52:43	−0.25836	103.0436	8	noaa20	1125	Batang Tuaka	Indragiri Hilir	Riau	Cluster
3	3 March 2020	00:52:43	−0.39327	102.9552	8	noaa20	1500	Tempuling	Indragiri Hilir	Riau	Cluster
4	3 March 2020	13:30:53	1.926316	101.4626	8	noaa20	1125	Rupat	Bengkalis	Riau	Cluster
5	3 March 2020	00:52:43	1.927811	101.4431	8	noaa20	2968	Rupat	Bengkalis	Riau	Cluster
6	3 March 2020	01:45:21	1.920925	101.4551	8	snpp	2769	Rupat	Bengkalis	Riau	Cluster
7	3 March 2020	01:45:21	1.966086	101.556	8	snpp	1668	Rupat Utara	Bengkalis	Riau	Cluster
8	3 March 2020	01:45:21	1.058746	102.953	8	snpp	1810	Tebing Tinggi	Kepulauan Meranti	Riau	Cluster
9	3 March 2020	01:45:21	1.090938	102.9439	8	snpp	1742	Tebing Tinggi	Kepulauan Meranti	Riau	Cluster
10	3 March 2020	01:45:21	0.995505	102.2071	8	snpp	2384	Sungai Apit	Siak	Riau	Cluster

Figure 5 presents the proportion of field fire incidents identified by two different types of hotspots (point and cluster), along with the connections to burned areas and peatlands. The following subsection elaborates on these findings.

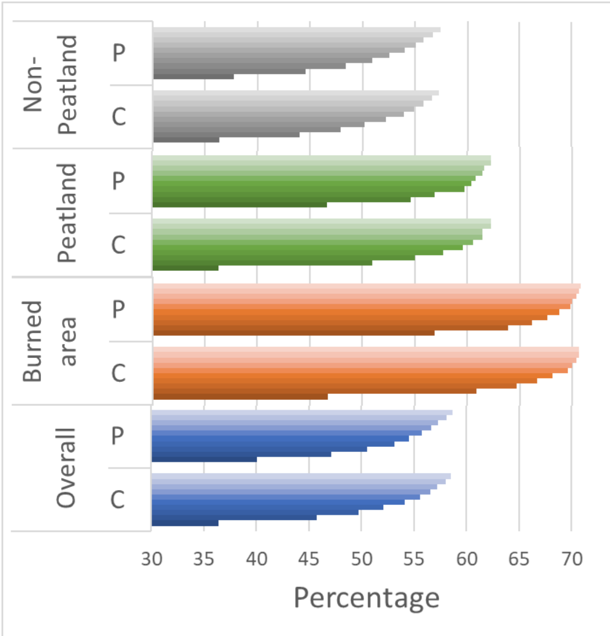

Figure 5. The percentage of field fire events accurately detected by two different types of hotspots (cluster (C) and point (P) hotspots) in connection to areas identified as burned on the burned map and the fire events found in peatlands or non-peatlands only. The dark-to-light shift in the shades of the colors represents the hotspot buffer range (from 375 m to ~4 km).

The total data evaluation comprised 1881 field points, 145,839 point-HS, and 98,188 cluster-HS, which means cluster-HS reduced the number of point-HS by up to 32.67%.

A comparison with field data showed that for both clustered- and point based hotspots, the accuracy increases at a buffer radius four times the size of the pixel VIIRS or around 1.5 km from the center of the fire (see Figure 6). Beyond a 1.5 km radius, these two types of hotspots no longer show a significant increase in accuracy.

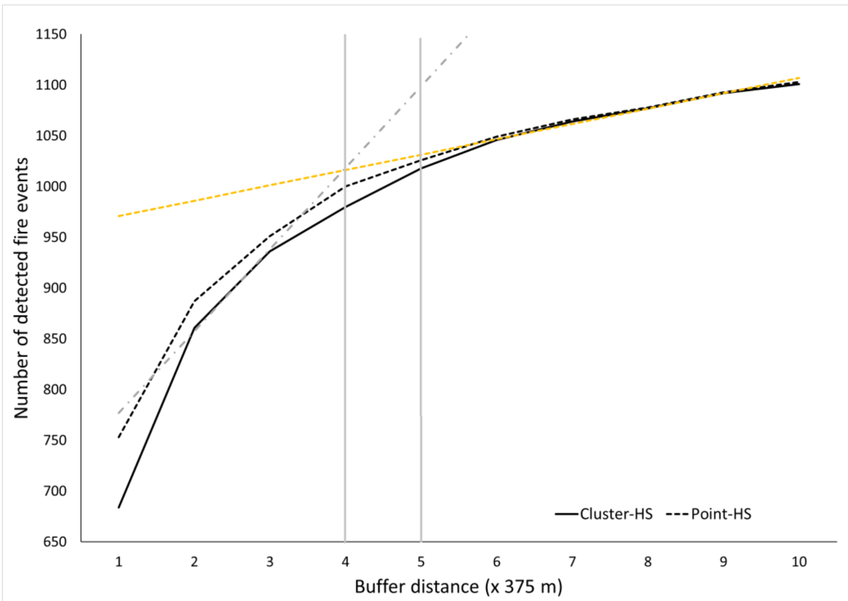

Figure 6. Assessment of cluster- and point-HS concerning the buffer distance. The x- and y-axes represent the buffer distance and the number of detected fire incidents, respectively. The two regression lines represent distinct slopes, with one being steep (yellow dashed line) and the other sloping (gray dashed line). The lines are perpendicular to the gray vertical line at buffer distance 4, indicating the optimal buffer distance for the number of detected fire events.

Our assessment of cluster-based and point-based hotspots concerning the buffer distance revealed that the distinction between point- and cluster-HS becomes negligible after exceeding 4 VIIRS pixels (equivalent to 1500 m). The gray vertical line in Figure 6 indicates the point of intersection between the two regression lines (yellow and gray dashed lines), which show the optimal buffer distance for achieving high accuracy in detecting actual fire incidents. However, as the saturation occurs beyond 5 VIIRS pixels (equivalent to 1875 m), it is recommended to look for fires within a radius of 5 pixels (less than 2 km) from the center of any fires, based on the cluster-HS point, for field verification.

Our findings indicate that most cluster-HS (95%) of all identified fire occurrences (Figure 7) were detected at a medium confidence level (CL = 8). Meanwhile, only around 2% were discovered at a high confidence level (CL = 9). These were found for all buffer distances from 375 to 3750 m.

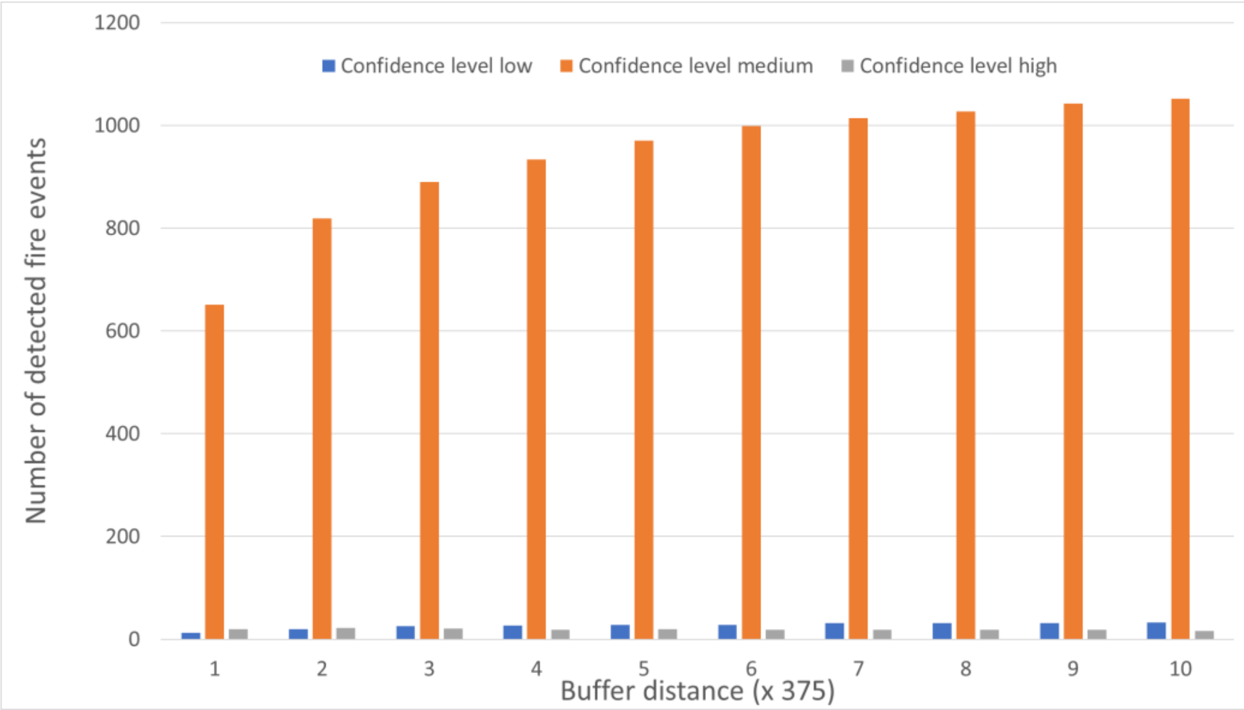

Figure 7. Overall results for clustered-based hotspots (cluster-HS) in terms of confidence levels.

3.2. The Validation of the Clustered- and Point-Based Hotspots and their Relationship with Burned Areas

Out of the 1881 fire points recorded in the field data, 473 of them coincide with the burned area data provided by the Ministry of Environment and Forestry. Out of the total of 473 points, only 22 points fall inside the radius of the buffer distance at 375 m. We discovered that by multiplying the buffer distance by four, the pixel size of VIIRS-375 (1500 m), the number of reported fire spots, and their overlap with the burned area grew by 20%. Notably, there was a substantial 16% increase between the first and second buffer distances. The significance of this rise diminishes after the fourth buffer (see Figure 8).

Above the buffer distance that is 5 times pixel size of VIIRS-375, cluster-HS and point-HS no longer differ significantly in accuracy beyond this distance (Figure 8). This demonstrates that cluster hotspots will be highly effective and practical for conducting field inspections within distances that are five times the size of the VIIRS pixel radius from the fire center (less than 2 km).

3.3. Clustered- and Point-Based Hotspot Validation with Peatlands and Non-Peatlands

Our analysis revealed that the accuracy varied more substantially in peatland areas compared to non-peatland areas for both the point-HS and cluster-HS hotspots (Figure 5).

The point-HS variants range from 46% to 62%, while the cluster-HS variations range from 36% to 62%. On non-peatlands, the discrepancy in precision remains very consistent for both types of hotspots across all distances. The discrepancy is minimal, approximately 0–1%, in terms of point-HS and cluster-HS in non-peatland areas. Differences in precision associated with this buffer distance were observed in fires located on peatlands, despite the fact that fires on peatlands account for just 25% of the field data. However, the precision in identifying peatland areas can be considerably improved to detection rate of up to 62%, compared to that of non-peatland areas, for which only a detection rate of 57% was obtained (see Figure 9).

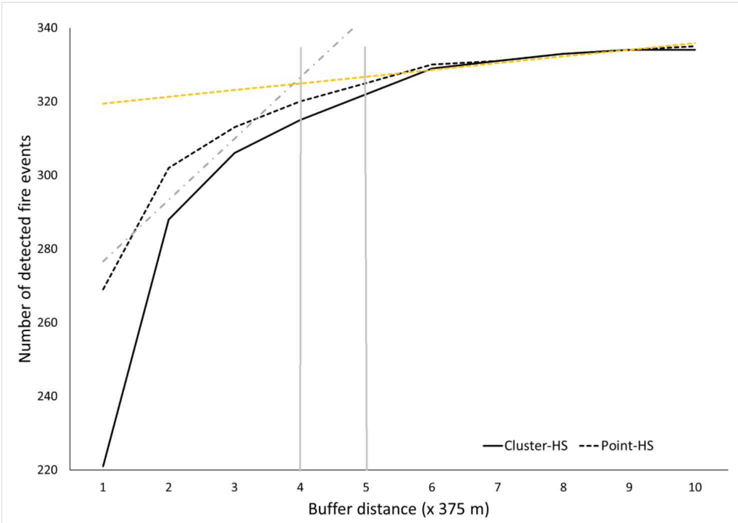

Figure 8. The assessment of clustered- and point-based hotspots in relation to the burned area map. The gray vertical line in buffer distance 4 shows the optimal point for the number of detected fire events (see also the two perpendicular regression lines) before being saturated at buffer size 5. In buffer 5, both types of hotspots no longer show a significant difference in the number of detected events. The first slope line is from buffer distance 1 to 4 (yellow dashed line), and the second is from buffer distance 5 to 10 (gray dashed line). The gray vertical line in buffer distance 5 shows that the difference between point-HS and cluster-HS is no longer significant after this line.

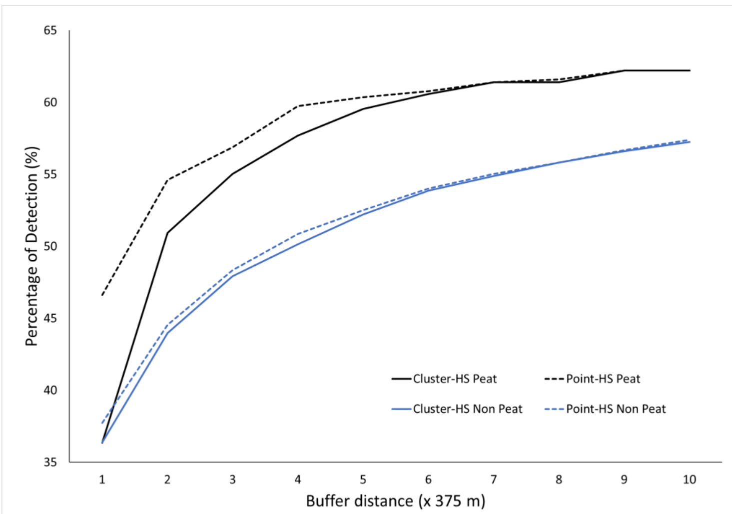

Figure 9. Percentage of detection (*POD*) fire events correctly detected by hotspots in peatland and non-peatland areas. The black line represents peatland areas; the blue line represents non-peatland areas. The dashed line represents point-based hotspot data (point-HS); the solid line represents clustered-based hotspot data (cluster-HS).

3.4. Clustered-Based Hotspot Assessment in Relation to Estimated Fire Size

The accuracy of hotspot detection in both peatland and non-peatland areas is highly influenced by the size of the fire, as shown in Figure 10. Typically, a fire size greater than 14 hectares (or the size of 1 pixel of VIIRS-375 image) has the highest level of accuracy, reaching up to 83%. For small fires (with a size of 3.5 hectares or less), the accuracy is greater in non-peatland areas compared to peatland areas. Additionally, Figure 10c displays suggestions for inspecting non-peat land, with a recommended radius of five times the pixel size (<2 km). Unlike peatland, non-peatland areas show a substantial increase in accuracy when the buffer distance is three times the pixel size (approximately 1 km).

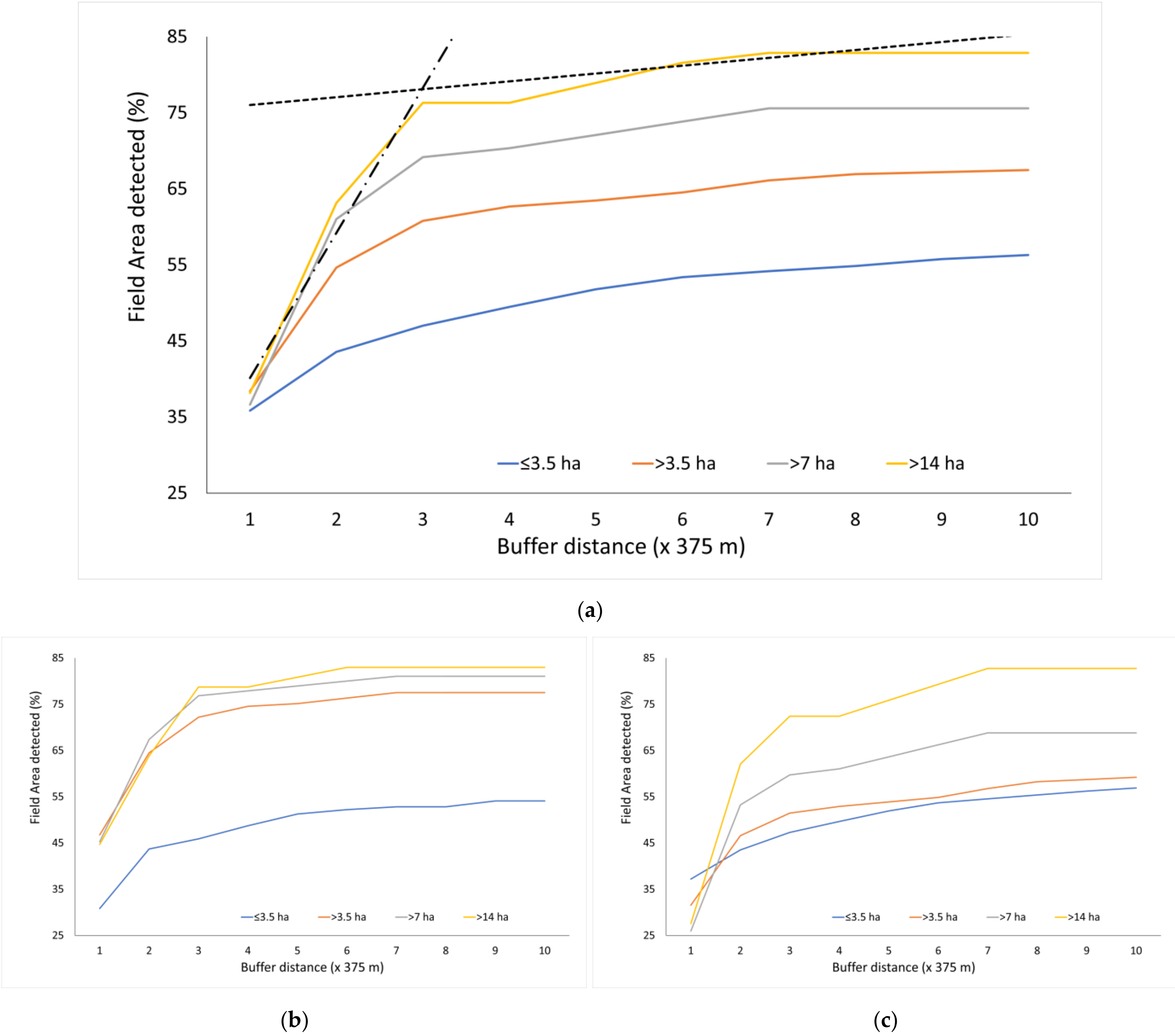

Figure 10. Cluster-HS assessment in relation to estimated fire size in: (**a**) all types of land; (**b**) peatland areas only; (**c**) non-peatland areas only. The two regression lines represent distinct slopes, with one being steep (dashed dot line) and the other sloping (dashed line).

4. Discussion

Previous research on peatland areas in Kalimantan and Sumatra is more varied than that for these locations' non-peatland areas [67]. The results for fire detection (*POD*), as presented in Figure 9, are also similar to a previous study, in which better performance for peatland areas than non-peatland was observed. However, the *POD* values over peatland areas have more variation than those for non-peatland areas. This could mean that fire detection in peatland areas is more challenging.

The results show that both point-HS and cluster-HS range from 52 to 53% *POD*, proving superior when compared to the results reported in a study in Heilongjiang province, China. This study, for comparison purposes, used field data, as was the case in the present study. In the above-mentioned study, VIIRS-375 data could detect no more than 30% *POD* [68]. This also shows that the global algorithm has a better ability to detect forest and land fires in Indonesia. In a study conducted on the Provinces of Riau and Central Kalimantan, the results showed that 71% of the field data could be detected by the VIIRS-375 hotspot [66]. Though the results of the present study, which covered the entire territory of Indonesia by 52% and 53% for cluster-HS and point-HS in general, look much smaller than the results of the study conducted on the Provinces of Riau and Central Kalimantan, it is important to note that study was only conducted on peatland areas. In our study, the results were pertained to peatland areas throughout Indonesia, showing a detection ability of 59 and 60% for cluster-HS and point-HS. This is due to the vast territory of Indonesia, the regions of which have several different characteristics. If we consider the estimated burn area from the field data, the *POD* can reach up to 83% for burn distances more than 14 ha.

A previous study that compared VIIRS-375 data with Landsat-8 data showed that fire areas spanning more than 14 ha have better results than those spanning less than 14 ha [63]. This is in accordance with the results of this study, possibly due to the pixel size of VIIRS-375, which is 375 m, forming an area of 140,725 m^2, or around 14 ha. This makes it easier to detect fires with an area of more than 14 ha. This was also confirmed by the HS-cluster, which showed a *POD* of 83%, i.e., the best performance.

Indonesia already has a national hotspot information monitoring system; the system runs in near-real-time with the time it takes for data to be received at a ground station for 30 min [60]. The clustering method has been used in the monitoring system since 2020 [33]. The cluster-HS method can reduce the amount of hotspot information by up to 67% [33] after previously masking hotspot data so that this number is closer to fire events, which makes it easier for field workers to conduct ground checking and is effective in using resources in the field.

Figure 11a shows the large fires that occurred in the Riau Province, which were detected with 96 point-HS, while the data from cluster-HS consisted of 5 points, and the field data reported consisted of 3 points. Figure 11b shows that only 1 fire incident was reported. The incident should be smaller than the 1-pixel size of VIIRS (375 m), so there was only 1 point-HS and 1 cluster-HS that shared the same location. Figure 11c shows fires detected by 3 point-HS, and the cluster-HS is shown by 1 point cluster-HS, which originates from the 3 point-HS, while the reported fire incident is also 1 point. Figure 11d shows that there were 2 adjacent fire incidents reported but that there was only 1 point-HS and 1 cluster-HS at the exact same location. This is possible because the distance between the two adjacent fire incidents is not more than one times of the VIIRS pixel size. The several samples above show that for fire events with small areas, the information from cluster-HS is almost the same as the information from point-HS. Thus, it can be seen that for large fire incidents, cluster-HS is better in terms of determining the number of fires than point-HS. This information can help the fire manager to locate the ongoing fire incidents. Simplifying the number of fire incidents that must be extinguished or checked by field officers or fire managers will speed up and facilitate coordination in the field. A smaller number of hotspots will also require less resources to check. Moreover, the intended location is relatively difficult to reach. However, for fires that are quite extensive, point-HS information will tend to be overestimated, while the cluster-HS information is closer to the number of real locations in the field. Those samples show the benefits of cluster-HS, particularly in the context of large fire events.

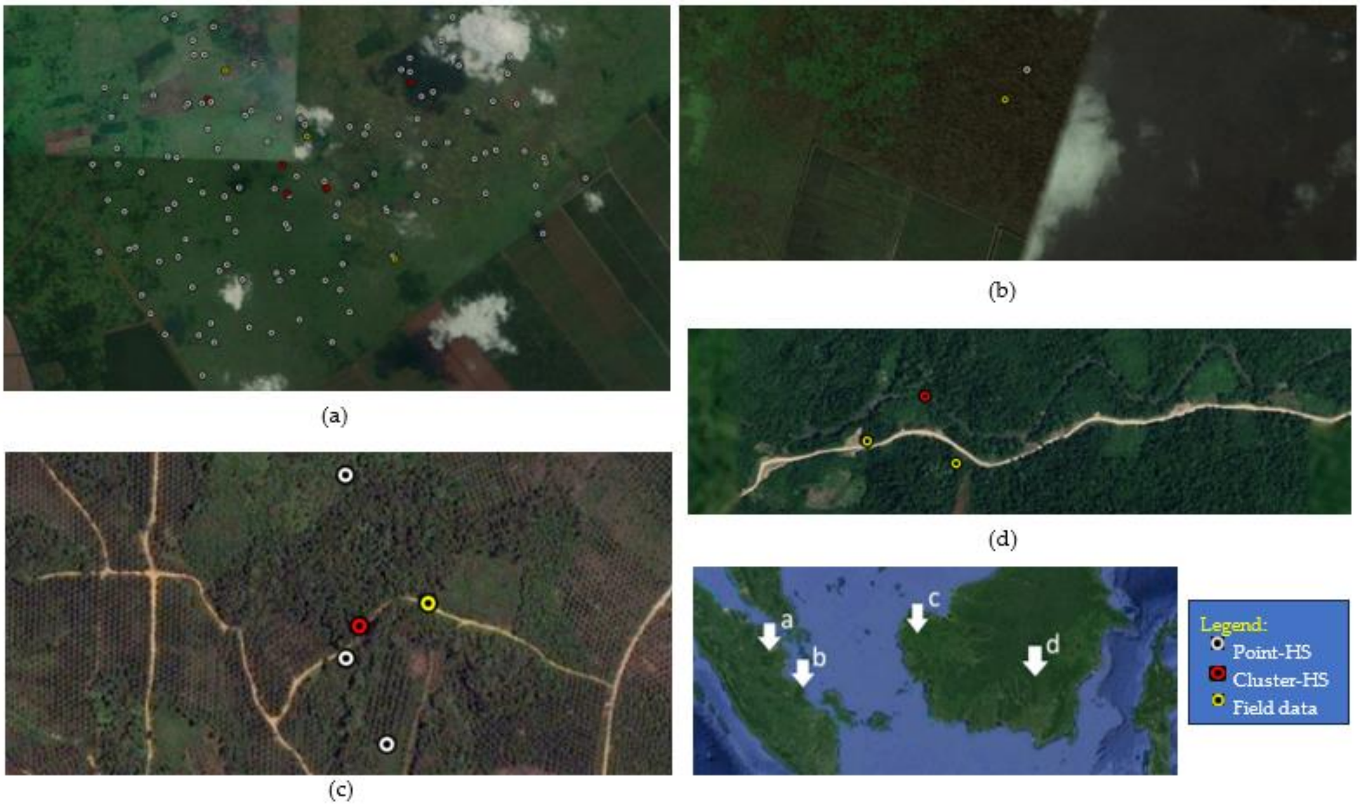

Figure 11. Example of cluster-HS vs. point-HS. Incident reported on 4 March 2020 in Riau Province (hotspot data from 3 March 2020) (**a**), incident reported on 6 March 2020 in South Sumatra Province (hotspot data from 6 March 2020) (**b**), incident reported on 15 August 2020 in West Kalimantan Province (hotspot data from 14 August 2020), (**c**) and incident reported on 23 August in Central Kalimantan Province (hotspot data from 22 August 2020) (**d**). The base map was made using data from Google Earth.

The availability of field data appears to influence the accuracy of the clustering algorithm outcomes. There were no documented fire occurrences in one sample in Central Sulawesi (Figure 12), but the point-HS data contained four points, and the cluster-HS contained one point originating from these four places. There were no field data or field officers to check on the fire at this location. If this method is used in areas/locations with limited field data, the results will be inaccurate or misleading. Based on the description above, the clustering method's strength is very good for use in the fire-prone areas of Indonesia, such as Kalimantan and Sumatra. Because forest/land fire management is more intensive in these two areas, officers frequently conduct field checks. The cluster method's output also helps with forest/land fire management by providing more precise information on the number of locations. The cluster method's weakness is that it is unsuitable for use in areas with little or no field data.

Indonesia has data on the calculation of the burned area (issued by the Ministry of Environment and Forestry). The data use medium-resolution satellite data (Landsat 8/9 and Sentinel 2) which uses a maximum distance of the pixel hotspot from the burn area that is 1.5 times the pixel hotspot size, while this study shows that the best buffer is 4 times the pixel size. This could be the consideration needed to make the maximum pixel hotspot distance 4 times the pixel size.

In the case of small fires (less than 6.25 ha, which is the minimum size of a burned area product), probably, the government has not thoroughly mapped the actual extent of the fire, as recorded in the field data. This problem frequently arises when Landsat (the primary dataset employed by the Indonesian government) or other medium-resolution images are used due to the images' spectral or spatial resolution limitations [69].

Figure 12. Example of cluster-HS vs. point-HS without a field report, as the incident was not reported in Central Sulawesi Province (hotspot data from 11 March 2020). The base map was made using data from Google Earth.

With the cluster-HS information, the fire manager can prioritize hotspot information originating from data in which clusters consisting of more than 1 point-HS have a greater possibility than clusters-HS which only originate from 1 point. To see if the data come from more than 1 pixel, one case use radius of possibility results; that is, if the radius of possibility value is greater, the data must come from more points.

Based on the results of the confidence level, it appears that only a small percentage (around 2%) have a high confidence level ($CL = 9$). This suggests that focusing on field checking does not align with a high confidence level. The confidence level of the generated hotspot information also has different detection variations on the surrounding object being detected [56], meaning that use in the field for prioritizing a high level of confidence becomes less relevant. This suggests that it would be advisable to include the use of a medium-confidence level product for field checking.

The aim of our study was to propose an improved approach for monitoring fires by using the clustering Euclidean method to derive cluster-based VIIRS hotspots in both peatlands and non-peatlands in Indonesia. This approach is straightforward but yields accuracy that is comparable to the current point-based hotspot method (without clustering), especially for burning detected within a radius of less than 2 km from the fire's center.

Daily hotspot information can be easily incorporated into daily operations throughout all regions of Indonesia due to the simplicity of the Euclidean distance clustering method. Monitoring vast fire areas will be simplified by the clustering method, as field officers will only receive a single data point for that area, as opposed to the multiple points that point-HS previously received. This will facilitate the identification of the specific locations that require inspection for forest fire management. The clustering method is particularly effective when applied to fire-prone regions of Indonesia, such as Kalimantan and Sumatra, where regular field checks are conducted. The clustering approach is not applicable, however, in places with limited or nonexistent field data, which is its main drawback.

In general fire products, the information usually contains coordinates of fire locations based on fire point number. The larger the area of fire occurrence, the higher the number of fire coordinates. Improvements in fire monitoring could lead to better, quicker responses for field checking and fire distinguishment efforts in the field.

The shortcomings of the clustering method have been identified, and they include the following: The hotspot data used in clustering method come from using the active fire global algorithm, which has its own shortcomings that come from clouds, water bodies, sun glints, semitransparent clouds, and bright objects [56]. Clustering methods are not superior to small fires because the detected fire may consist of only one point (or even missing fires). Clustering methods are not ideal for small fires because the detected fire may only be a single point or may not be present at all. In this instance, no benefit was gained.

5. Conclusions

The Clustering Euclidean distance method is simple and achieves nearly the same accuracy as the point method (without clustering), particularly in buffering areas that are more than five times the pixel resolution. It also resulted in a reduction of up to 32.67% in the number of hotspots.

The cluster-HS and point-HS methods for VIIRS data both achieved the highest level of accuracy when the buffering area was four times the pixel resolution (1.5 km), resulting in validation rates of 52% and 53%, respectively. The hotspot information obtained from the VIIRS sensor offered highly accurate information for the hotspots, particularly for areas larger than 14 hectares, with an accuracy rate of up to 83%.

Cluster-HS exhibits superior performance in peatland areas rather than non-peatland areas. It accuracy can reach up to 62% for peatland areas (compared to 57% on non-peatland areas), but there is greater variation for peatland areas. In a small buffer, the cluster-HS accuracy could differ by up to 10% for peatland areas, while for non-peatland areas, it is only 1%.

The benefit of the Euclidean distance clustering method is its simplicity, since it could produce daily hotspot information which can be easily incorporated into daily operations throughout all regions of Indonesia. However, the clustering approach is not applicable in places with limited or nonexistent field data, which is its main drawback.

Author Contributions: Conceptualization, methodology, software, data processing, validation, formal analysis, investigation, writing—original draft preparation, A.I.; analysis, writing—review and editing, M.D., Y.V., E.S.A. and R.R.; visualization, A.I. and Y.V.; supervision, M.D., E.S.A. and R.R. All authors have read and agreed to the published version of the manuscript.

Funding: This research is funded by University of Indonesia, through Hibah PUTI Q2 2023–2024 via grant letter number NKB-755/UN2.RST/HKP.05.00/2023.

Institutional Review Board Statement: Not applicable.

Informed Consent Statement: Not applicable.

Data Availability Statement: The Data Fire hotspots used in this study are accessible via https://hotspot.brin.go.id/ (accessed on 1 August 2023). Data can be viewed and downloaded from this website. The method proposed in this study is also used on this site. Field data and burn area maps were received from the Ministry of Forestry and Environment and used exclusively for this study.

Acknowledgments: BRIN provided facilities and scholarships for this research. University of Indonesia provided the necessary educational facilities and publication funds. Additionally, the Ministry of Forestry and the Environment provided reference data. We acknowledge Wismu Sunarmodo for his assistance in software preparation.

Conflicts of Interest: The authors declare that there are no conflicts of interest regarding the publication of this paper.

References

1. Jeannette Glauber, A.; Moyer, S.; Adriani, M.; Gunawan Elitza Mileva, I.; Harimurti, P.; Farman Izhar, M.; Kendrick, A.; Henry Stirrett Wood, G. The Cost of Fire: An Economic Analysis of Indonesia's 2015 Fire Crisis. The World Bank Indonesia Stock Exchange Building, Tower 2, 12th floor Jl. 2016. Available online: http://hdl.handle.net/10986/23840 (accessed on 1 August 2023).
2. Show, D.L.; Chang, S. Atmospheric impacts of Indonesian fire emissions: Assessing remote sensing data and air quality during 2013 Malaysian haze. *Procedia Environ. Sci.* **2016**, *36*, 176–179. [CrossRef]
3. Kaskaoutis, D.G.; Kumar, S.; Sharma, D.; Singh, R.P.; Kharol, S.K.; Sharma, M.; Singh, A.K.; Singh, S.; Singh, A.; Singh, D. Effects of crop residue burning on aerosol properties, plume characteristics, and long-range transport over northern India. *J. Geophys. Res.* **2014**, *119*, 5424–5444. [CrossRef]

4. Singh, P.; Dey, S. Crop burning and forest fires: Long-term effect on adolescent height in India. *Resour. Energy Econ.* **2021**, *65*, 101244. [CrossRef]
5. Rangel, M.A.; Vogl, T. *Agricultural Fires and Infant Health*; Working Paper 22955; National Bureau Of Economic Research: Cambridge, MA, USA, 2016. [CrossRef]
6. Rosales-Rueda, M.; Triyana, M. The Persistent Effects of Early-Life Exposure to Air Pollution: Evidence from the Indonesian Forest Fires. *J. Hum. Resour.* **2019**, *54*, 1037–1080. [CrossRef]
7. Tan-Soo, J.S.; Pattanayak, S.K. Seeking natural capital projects: Forest fires, haze, and early-life exposure in Indonesia. *Proc. Natl. Acad. Sci. USA* **2019**, *116*, 5239–5245. [CrossRef] [PubMed]
8. Endrawati, E.; Purwanto, J.; Nugroho, S.; Agung, R. Identifikasi Areal Bekas Kebakaran Hutan Dan Lahan Menggunakan Analisis Semi Otomatis Citra Satelit LANDSAT. *Semin. Nas. Geomatika* **2017**, *2*, 273–282. [CrossRef]
9. Indradjad, A.; Purwanto, J.; Sunarmodo, W. Analisis Tingkat Akurasi Titik Hotspot Dari S-NPP VIIRS Dan Terra/Aqua MODIS Terhadap Kejadian Kebakaran (Accuracy Analysis of Hotspots from S-NPP VIIRS and Terra/Aqua MODIS to Fire Occurrences). *J. Penginderaan Jauh dan Pengolah. Data Citra Digit.* **2019**, *16*, 53–60.
10. Atwood, E.C.; Englhart, S.; Lorenz, E.; Halle, W.; Wiedemann, W.; Siegert, F. Detection and Characterization of Low Temperature Peat Fires during the 2015 Fire Catastrophe in Indonesia Using a New High- Sensitivity Fire Monitoring Satellite Sensor (FireBird). *PLoS ONE* **2016**, *11*, e0159410. [CrossRef]
11. Xie, Z.; Song, W.; Ba, R.; Li, X.; Xia, L. A spatiotemporal contextual model for forest fire detection using Himawari-8 satellite data. *Remote Sens.* **2018**, *10*, 1992. [CrossRef]
12. Plank, S.; Fuchs, E.M.; Frey, C. A fully automatic instantaneous fire hotspot detection processor based on AVHRR imagery-A TIMELINE thematic processor. *Remote Sens.* **2017**, *9*, 30. [CrossRef]
13. Xu, W.; Wooster, M.J.; He, J.; Zhang, T. Improvements in high-temporal resolution active fire detection and FRP retrieval over the Americas using GOES-16 ABI with the geostationary Fire Thermal Anomaly (FTA) algorithm. *Sci. Remote Sens.* **2021**, *3*, 100016. [CrossRef]
14. Li, F.; Zhang, X.; Kondragunta, S.; Schmidt, C.C.; Holmes, C.D. A preliminary evaluation of GOES-16 active fire product using Landsat-8 and VIIRS active fire data, and ground-based prescribed fire records. *Remote Sens. Environ.* **2020**, *237*, 111600. [CrossRef]
15. Fuchs, E.-M.; Stein, E.; Strunz, G.; Strobl, C.; Frey, C. Fire Monitoring—The use of medium resolution satellites (AVHRR, MODIS, TET) for long time series processing and the implementation in User Driven Applications and Services. *ISPRS Int. Arch. Photogramm. Remote Sens. Spat. Inf. Sci.* **2015**, *XL7*, 797–804. [CrossRef]
16. Giglio, L.; Schroeder, W.; Justice, C.O. The collection 6 MODIS active fire detection algorithm and fire products. *Remote Sens. Environ.* **2016**, *178*, 31–41. [CrossRef] [PubMed]
17. Giglio, L.; Descloitres, J.; Justice, C.O.; Kaufman, Y.J. An Enhanced Contextual Fire Detection Algorithm for MODIS. *Remote Sens. Environ.* **2003**, *87*, 273–282. [CrossRef]
18. Csiszar, I.; Schroeder, W.; Giglio, L.; Ellicott, E.; Vadrevu, K.P.; Justice, C.O.; Wind, B. Active fires from the Suomi NPP Visible Infrared Imaging Radiometer Suite: Product status and first evaluation results. *J. Geophys. Res. Atmos. Res.* **2014**, *119*, 803–816. [CrossRef]
19. Elvidge, C.D.; Zhizhin, M.; Hsu, F.C.; Sparks, T.; Ghosh, T. Subpixel analysis of primary and secondary infrared emitters with nighttime viirs data. *Fire* **2021**, *4*, 83. [CrossRef]
20. Elvidge, C.D.; Zhizhin, M.; Hsu, F.C.; Baugh, K.E. VIIRS nightfire: Satellite pyrometry at night. *Remote Sens.* **2013**, *5*, 4423–4449. [CrossRef]
21. Oliva, P.; Schroeder, W. Assessment of VIIRS 375 m active fire detection product for direct burned area mapping. *Remote Sens. Environ.* **2015**, *160*, 144–155. [CrossRef]
22. Briones-Herrera, C.I.; Vega-Nieva, D.J.; Monjarás-Vega, N.A.; Briseño-Reyes, J.; López-Serrano, P.M.; Corral-Rivas, J.J.; Alvarado-Celestino, E.; Arellano-Pérez, S.; Álvarez-González, J.G.; Ruiz-González, A.D.; et al. Near real-time automated early mapping of the perimeter of large forest fires from the aggregation of VIIRS and MODIS active fires in Mexico. *Remote Sens.* **2020**, *12*, 2061. [CrossRef]
23. Alonso-canas, I.; Chuvieco, E. Global burned area mapping from ENVISAT-MERIS and MODIS active fi re data. *Remote Sens. Environ.* **2015**, *163*, 140–152. [CrossRef]
24. Giglio, L.; Boschetti, L.; Roy, D.P.; Humber, M.L.; Justice, C.O. The Collection 6 MODIS burned area mapping algorithm and product. *Remote Sens. Environ.* **2018**, *217*, 72–85. [CrossRef] [PubMed]
25. Marsha, A.L.; Larkin, N.K. Evaluating Satellite Fire Detection Products and an Ensemble Approach for Estimating Burned Area in the United States. *Fire* **2022**, *5*, 147. [CrossRef]
26. Schroeder, W.; Oliva, P.; Giglio, L.; Quayle, B.; Lorenz, E.; Morelli, F. Active fire detection using Landsat-8/OLI data. *Remote Sens. Environ.* **2016**, *185*, 210–220. [CrossRef]
27. Kumar, S.S.; Roy, D.P. Global operational land imager Landsat-8 reflectance-based active fire detection algorithm. *Int. J. Digit. Earth* **2018**, *11*, 154–178. [CrossRef]
28. Liu, T.; Mickley, L.J.; Marlier, M.E.; DeFries, R.S.; Khan, M.F.; Latif, M.T.; Karambelas, A. Diagnosing spatial biases and uncertainties in global fire emissions inventories: Indonesia as regional case study. *Remote Sens. Environ.* **2020**, *237*, 111557. [CrossRef]

29. Xiang, M.; Xiao, C.; Feng, Z.; Ma, Q. Global distribution, trends and types of active fire occurrences. *Sci. Total Environ.* **2023**, *902*, 166456. [CrossRef]
30. Sofan, P.; Yulianto, F.; Sakti, A.D. Characteristics of False-Positive Active Fires for Biomass Burning Monitoring in Indonesia from VIIRS Data and Local Geo-Features. *ISPRS Int. J. Geo-Inf.* **2022**, *11*, 601. [CrossRef]
31. Caseiro, A.; Rücker, G.; Tiemann, J.; Leimbach, D.; Lorenz, E.; Frauenberger, O.; Kaiser, J.W. Persistent hot spot detection and characterisation using SLSTR. *Remote Sens.* **2018**, *10*, 1118. [CrossRef]
32. Liu, Y.; Hu, C.; Zhan, W.; Sun, C.; Murch, B.; Ma, L. Identifying industrial heat sources using time-series of the VIIRS Nightfire product with an object-oriented approach. *Remote Sens. Environ.* **2018**, *204*, 347–365. [CrossRef]
33. Indradjad, A.; Sumnarmodo, W.; Adiningsih, E.S.; Dimyati, M.; Rokhmatuloh. Fire-hotspot information system from multi-resolution remote sensing data for early detection of forest fires. In Proceedings of the ACRS 2020—41st Asian Conference on Remote Sensing, Deqing City, China, 9–11 November 2020; pp. 538–545.
34. Syaufina, L.; Sitanggang, I.S. Peatland fire detection using spatio-temporal data mining analysis in Kalimantan, Indonesia. *J. Trop. For. Sci.* **2018**, *30*, 154–162. [CrossRef]
35. Di Martino, F.; Sessa, S. Extended Fuzzy C-Means hotspot detection method for large and very large event datasets. *Inf. Sci.* **2018**, *441*, 198–215. [CrossRef]
36. Chart-Asa, C. Spatial-temporal patterns of MODIS active fire/hotspots in Chiang Rai, upper northern Thailand and the greater mekong subregion countries during 2003–2015. *Appl. Environ. Res.* **2021**, *43*, 121–131. [CrossRef]
37. Lizundia-Loiola, J.; Otón, G.; Ramo, R.; Chuvieco, E. A spatio-temporal active-fire clustering approach for global burned area mapping at 250 m from MODIS data. *Remote Sens. Environ.* **2020**, *236*, 111493. [CrossRef]
38. Humber, M.L.; Boschetti, L.; Giglio, L.; Justice, C.O. Spatial and temporal intercomparison of four global burned area products. *Int. J. Digit. Earth* **2019**, *12*, 460–484. [CrossRef] [PubMed]
39. Butar-Butar, K.D.; Zamzami, E.M.; Damanik, N.; Rikki, A.; Darlina, E. Spatial Distribution and Implementation of the K-Means Clustering Method at Hotspots in North Sumatra. *J. Comput. Phys. Earth Sci.* **2021**, *1*, 1–6. [CrossRef]
40. Setiawan, Y.; Prasetyo, L.B.; Pawitan, H.; Permatasari, P.A.; Suyamto, D.; Wijayanto, A.K. Identifying Areas Affected By Fires in Sumatra Based on Time Series of Remotely Sensed Fire Hotspots and Spatial Modeling. *J. Pengelolaan Sumberd. Alam Lingkung. (J. Nat. Resour. Environ. Manag.)* **2018**, *8*, 420–427. [CrossRef]
41. Cizungu, N.C.; Tshibasu, E.; Lutete, E.; Mushagalusa, C.A.; Mugumaarhahama, Y.; Ganza, D.; Karume, K.; Michel, B.; Lumbuen-amo, R.; Bogaert, J. Fire risk assessment, spatiotemporal clustering and hotspot analysis in the Luki biosphere reserve region, western DR Congo. *Trees For. People* **2021**, *5*, 100104. [CrossRef]
42. Di Martino, F.; Sessa, S. The extended fuzzy C -means algorithm for hotspots in spatio-temporal GIS. *Expert Syst. Appl.* **2011**, *38*, 11829–11836. [CrossRef]
43. Kurniawan, M.; Muhima, R.R.; Agustini, S. Comparison of Clustering K-Means, Fuzzy C-Means, and Linkage for Nasa Active Fire Dataset. *Int. J. Artif. Intell. Robot.* **2020**, *2*, 34–41. [CrossRef]
44. Khairani, N.A.; Sutoyo, E. Application of K-Means Clustering Algorithm for Determination of Fire-Prone Areas Utilizing Hotspots in West Kalimantan Province. *Int. J. Adv. Data Inf. Syst.* **2020**, *1*, 9–16. [CrossRef]
45. Kirana, A.P.; Sitanggang, I.S.; Syaufina, L. Poisson Clustering Process on Hotspot in Peatland Area using Kulldorff's Scan Statistics Method. *TELKOMNIKA (Telecommun. Comput. Electron. Control)* **2015**, *13*, 1376. [CrossRef]
46. Wijaya, P.T.; Sitanggang, I.S.; Syaufina, L. Density based clustering of hotspots in peatland with road and river as physical obstacles. *Indones. J. Electr. Eng. Comput. Sci.* **2016**, *3*, 714. [CrossRef]
47. Hermawati, R.; Sitanggang, I.S. Web-Based clustering application using Shiny framework and DBSCAN algorithm for hotspots data in peatland in Sumatra. *Procedia Environ. Sci.* **2016**, *33*, 317–323. [CrossRef]
48. Usman, M.; Sukaesih, I.; Syaufina, L. Hotspot distribution analyses based on peat characteristics using density-based spatial clustering. *Procedia Environ. Sci.* **2015**, *24*, 132–140. [CrossRef]
49. Anwar, M.T.; Hadikurniawati, W.; Winarno, E.; Supriyanto, A. Wildfire Risk Map Based on DBSCAN Clustering and Cluster Density Evaluation. *Adv. Sustain. Sci. Eng. Technol.* **2019**, *1*, 0190102. [CrossRef]
50. de Almeida Pereira, G.H.; Fusioka, A.M.; Nassu, B.T.; Minetto, R. Active fire detection in Landsat-8 imagery: A large-scale dataset and a deep-learning study. *ISPRS J. Photogramm. Remote Sens.* **2021**, *178*, 171–186. [CrossRef]
51. Waigl, C.F.; Stuefer, M.; Prakash, A.; Ichoku, C. Detecting high and low-intensity fires in Alaska using VIIRS I-band data: An improved operational approach for high latitudes. *Remote Sens. Environ.* **2017**, *199*, 389–400. [CrossRef]
52. Wooster, M.J.; Roberts, G.J.; Giglio, L.; Roy, D.; Freeborn, P.; Boschetti, L.; Justice, C.; Ichoku, C.; Schroeder, W.; Davies, D.; et al. Satellite remote sensing of active fires: History and current status, applications and future requirements. *Remote Sens. Environ.* **2021**, *267*, 112694. [CrossRef]
53. Yang, X.; Hua, Z.; Zhang, L.; Fan, X.; Zhang, F.; Ye, Q.; Fu, L. Preferred vector machine for forest fire detection. *Pattern Recognit.* **2023**, *143*, 109722. [CrossRef]
54. Ying, L.; Han, J.; Du, Y.; Shen, Z. Forest fire characteristics in China: Spatial patterns and determinants with thresholds. *For. Ecol. Manag.* **2018**, *424*, 345–354. [CrossRef]
55. Bo, W.; Liu, J.; Fan, X.; Tjahjadi, T.; Ye, Q.; Fu, L. BASNet: Burned Area Segmentation Network for Real-time Detection of Damage Maps in Remote Sensing Images. *IEEE Trans. Geosci. Remote Sens.* **2022**, *60*, 1–13. [CrossRef]

56. Schroeder, W.; Oliva, P.; Giglio, L.; Csiszar, I.A. The New VIIRS 375 m active fire detection data product: Algorithm description and initial assessment. *Remote Sens. Environ.* **2014**, *143*, 85–96. [CrossRef]
57. Oudrari, H.; McIntire, J.; Xiong, X.; Butler, J.; Ji, Q.; Schwarting, T.; Lee, S.; Efremova, B. JPSS-1 VIIRS radiometric characterization and calibration based on pre-launch testing. *Remote Sens.* **2016**, *8*, 41. [CrossRef]
58. Huang, A.; Gumley, L.; Strabala, K.; Mindock, S.; Garcia, R.; Martin, G.; Cureton, G.; Davies, J.; Bearson, N.; Braum, J.; et al. Community Satellite Processing Package from Direct Broadcast: Providing real-time Satellite Data to every corner of the world. In Proceedings of the 2016 IEEE International Geoscience and Remote Sensing Symposium (IGARSS), Beijing, China, 10–15 July 2016; pp. 5532–5535. [CrossRef]
59. Gustiandi, B.; Indradjad, A. Visible Infrared Imager Radiometer Suite (VIIRS) Active Fires Application Related Products (AFARP) Generation Using Community Satellite Processing Package (CSPP) Software. In Proceedings of the 34th Asian Conference on Remote Sensing; Indonesian Remote Sensing Society and Asian Association on Remote Sensing, Bali, Indonesia, 20–24 October 2013; pp. SC02-893–SC02-900.
60. Indradjad, A.; Sunarmodo, W.; Salyasari, N.; Pratiknyo, B. Development of National Forest/Land Fire Monitoring System Using Remote Sensing Satellite Data (Terra/Aqua Modis and SNPP) by Automation and Nearly Real-time. *IOP Conf. Ser. Earth Environ. Sci.* **2019**, *280*, 012032. [CrossRef]
61. Ritung, S.; Wahyunto, N.K.; Sukarman, H.; Suparto, T.C. *Peta Lahan Gambut Indonesia Skala 1:250,000 (Indonesia Peat Soil Map 1:250,000)*; IAARD Press, Ministry of Agriculture, Agency for Agricultural Research and Development: Bogor, Indonesia, 2011.
62. Schroeder, W.; Prins, E.; Giglio, L.; Csiszar, I.; Schmidt, C.; Morisette, J.; Morton, D. Validation of GOES and MODIS active fire detection products using ASTER and ETM+ data. *Remote Sens. Environ.* **2008**, *112*, 2711–2726. [CrossRef]
63. Sofan, P.; Bruce, D.; Schroeder, W.; Jones, E.; Marsden, J. Assessment of VIIRS 375 m active fire using tropical peatland combustion algorithm applied to Landsat-8 over Indonesia's peatlands. *Int. J. Digit. Earth* **2020**, *13*, 1695–1716. [CrossRef]
64. Vetrita, Y.; Haryani, N.S. Validasi Hotspot MODIS INDOFIRE di Province Riau (Validation of MODIS INDOFIRE in Riau Province). *J. Ilm. Geomatika* **2012**, *18*, 17–28.
65. Çolak, E.; Sunar, F. The importance of ground-truth and crowdsourcing data for the statistical and spatial analyses of the NASA FIRMS active fires in the Mediterranean Turkish forests. *Remote Sens. Appl. Soc. Environ.* **2020**, *19*, 100327. [CrossRef]
66. Sofan, P.; Bruce, D.; Jones, E.; Marsden, J. Detection and validation of tropical Peatland flaming and smouldering using Landsat-8 SWIR and TIRS bands. *Remote Sens.* **2019**, *11*, 465. [CrossRef]
67. Vetrita, Y.; Cochrane, M.A. Fire frequency and related land-use and land-cover changes in Indonesia's Peatlands. *Remote Sens.* **2020**, *12*, 5. [CrossRef]
68. Jiao, Q.; Fan, M.; Tao, J.; Wang, W.; Liu, D.; Wang, P. Forest Fire Patterns and Lightning-Caused Forest Fire Detection in Heilongjiang Province of China Using Satellite Data. *Fire* **2023**, *6*, 166. [CrossRef]
69. Gaveau, D.L.A.; Descals, A.; Salim, M.A.; Sheil, D.; Sloan, S. Refined burned-area mapping protocol using Sentinel-2 data increases estimate of 2019 Indonesian burning. *Earth Syst. Sci. Data* **2021**, *13*, 5353–5368. [CrossRef]